# Simulating lithium deposition on planar anode: the role of particle reservoir and the influence of dendrite growth on current density profiles.

Paula V. Saravia,[†,‡] C. Andrea Calderón,[¶] Ezequiel P. M. Leiva,[†,‡] and S. Alexis Paz[*,†,‡]

†*Universidad Nacional de Córdoba. Facultad de Ciencias Químicas. Departamento de Química Teórica y Computacional, X5000HUA, Córdoba, Argentina.*

‡*Consejo Nacional de Investigaciones Científicas y Técnicas (CONICET), Instituto de Investigaciones en Fisicoquímica de Córdoba (INFIQC), X5000HUA, Córdoba, Argentina.*

¶*Consejo Nacional de Investigaciones Científicas y Técnicas (CONICET), Instituto de Física Enrique Gaviola (IFEG), X5000HUA, Córdoba, Argentina.*

E-mail: apaz@unc.edu.ar

**Abstract**

In this work, we developed a computational model of lithium deposition on planar electrodes. With this model, we simulated several chronoamperometry experiments considering different deposition probabilities, i.e. cell overpotentials. Since the planar geometry induces an ion concentration gradient profile that continues to evolve toward the bulk electrolyte, we studied the influence of the lithium reservoir and rationalized its role in the real system. The solid electrolyte interface (SEI) is conceptualized as a thin layer whose thickness determines the ion diffusion profile. Additionally, the impact of dendrite formations on electrode roughness and current density profiles was

analyzed by comparison with test simulations assuming inhibited dendrite growth. By presenting current density profiles in quantitatively meaningful units, our work narrows the gap for further comparison with experimental measurements. The utility of our simulations for determining the electrode area in lithium metal batteries is addressed.

# Introduction

Lithium metal is one of the most frequently used elements for the anode material in post-lithium ion energy storage systems due to its very high theoretical specific capacity ($3860\,\mathrm{mAhg^{-1}}$), the lowest redox potential ($-3.04\,\mathrm{V}$ vs. SHE) and a low gravimetric density ($0.534\,\mathrm{g\,cm^{-3}}$).[1,2] Among these technologies, we can mention Li-S and Li-Air.[3,4] However, one of the main issues under study with this electrode is the growth of metal dendrites on its surface during deposition. Such formations introduce safety and cyclability concerns, decreasing coulombic efficiency and provoking capacity fading.[5,6] Extensive research has been done to propose different strategies to control dendrite growth,[7,8] while trying to characterize the conditions under which dendrites occur. Computational studies are progressively contributing to these efforts.[9–13] Coarse-grained models are of great interest for studying the lithium metal interface during electrodeposition, as they allow exploration of longer space and time scales compared to full atomistic approaches. Given the mismatch between dendrite dimensions (approximately $\mu$m) and molecular size, the simplified representation of this system also becomes necessary to make the problem manageable.[14] Nevertheless, these models require further development to better represent the system and enable quantitative comparisons with experimental observations. Longer time scales are desired to properly describe experiments while maintaining the level of detail that the simulation allows. This detail is of great interest for the proper understanding of the nanoscale processes that lead to the onset of dendrite formation. At the spatial scale where electrodeposition occurs, it becomes relevant the SEI formation. With a finite thickness (5-50

nm), this interphase is formed on the bare Li metal surface when it makes contact with the electrolyte. Given the reactive nature of Li, the chemical composition of the SEI is not precisely characterized and depends on electrolyte composition.[15]

Mayers *et al.* have modeled $Li^+$ electrodeposition on a hemispherical electrode.[16] Their coarse-grained model enabled the simulation of long timescales (up to 400 ms), as well as length scales of interest associated with the onset of metal dendrite formation. They focused on how the application of time-dependent overpotential pulses to the electrode leads to the suppression of dendrite formation, due to the competition between timescales for cation diffusion and reduction at the anode/SEI interface. Pulse-charging techniques have also been analyzed by Aryanfar *et al.* in several studies.[17–19] In these other cases, electromigration was also considered, as well as thermal relaxation of the dendrites. Other models have been developed to study how the difference between the diffusion coefficients of the electrolyte and the SEI affects the structure of deposited Li. This is the case of the work by Byun *et al.*[20] The analysis of the SEI shape and flexibility, as well as other properties, is also of great interest, as the balance between SEI flexibility and hardness may be critical to avoid dendrite growth. On the other hand, the coarse-grained model by Kong *et al.* studied the effect of a polymer coating layer on Li deposition.[14] The presence of a rather flexible and thin interphase between the anode and the electrolyte favours homogeneous deposition, whether this interphase is the SEI or a polymeric coating.

Inspired by the previous reserch, we developed a model to simulate electrodeposition onto a planar electrode. The aim was to simulate a chronoamperometry experiment, characterizing current density profiles and other quantities, all presented in standard experimental units. Potentiostatic conditions were simulated by controlling the deposition probability $\rho$, which is directly related to the cell overpotential.[16] We introduced three novel features compared to previous works: we conceptualize the SEI as a thin layer whose thickness determines the ion diffusion profile; we assess dendrite influence by comparing it with inhibited deposition simulations; and account for cation-cation interactions using

a Hard Spheres model. The utility of our simulations for determining the electrode area in lithium metal batteries is discussed.

## Simulation Methods

The present model is based on that developed by Mayers *et al.*,[16] and with it, we simulated potentiostatic Li metal deposition. As a main difference from previous work, our model introduces a planar geometry resembling the most common experimental situation and considers a finite diffusion space representing the solid electrolyte interface (SEI). The simulation box is a cube with a length of 300 Å on each axis, as illustrated in Fig. 1. It is divided into a region comprising the electrode and the SEI, spanning from the implicit ideal electrode at z= 0 Å up to z= 280 Å. Then, between z= 280 Å and z= 300 Å the model introduces a Grand Canonical Monte Carlo (GCMC) reservoir,[21,22] which keeps the system at a constant chemical potential $\mu$ begins, as shown in Fig. 1. The working mechanism of this reservoir is detailed in the supporting information. The initial number of ions in the cell is set to yield a concentration of 1 M, which is the usual one in coin cells using $LiPF_6$ in carbonate based solvent as well other electrolytes.[23,24] This is adopted as the bulk concentration for all the present simulations.

Particles evolve according to Brownian dynamics, described by the following equation:[16]

$$r_i(t + \Delta t) = r_i(t) + (2D\Delta t)^{1/2} g_i \tag{1}$$

where $D$ is the diffusion coefficient, $\Delta t = 1$ ns is the time step, and $g_i$ is a random factor representing the fluctuating forces acting on a particle. We chose a value of $D = 2.5\ 10^{-14}$ $m^2/s$, which is in the same order of magnitude as the experimental diffusion coefficient of lithium ions in a SEI.[12] Periodic boundary conditions are imposed along the x and y cell directions. Following Mayers *et al.*, ionic migration and interaction with anions present in the solvent were not considered, assuming charge screening at short distances. Inter-

actions between cations are considered within the Hard Spheres (HS) model, setting a superposition radius of $r_{HS} = 3.2$ Å, as assumed in the work of Selis and Seminario.[12] Thus, whenever a pair of cations were closer than $r_{HS}$, resulting in particles overlapping, the position update step was rejected. The particle that caused the overlap returned to its previous position, resulting in no possible approach between cations in the SEI closer than $r_{HS}$. An electrodeposition event can occur stochastically with a probability of acceptance $\rho$, $(0< \rho <1)$, when the $Li^+$ ions are within a distance $r_{HS}$ from the implicit electrode or another deposited particle. Thus $r_{HS}$ is also considered as the electronic transfer (ET) distance, $r_{ET}$. The probability $\rho$ allows for the control of the electrodeposition event and in this model we can relate it to the change of overpotential applied to the Li electrode.[16] After a deposition event occurs, the particle position is kept fixed throughout the rest of the simulation, as from that moment on it is considered part of the electrode. In the case where the particle does not react, it bounces away from deposited Li or the electrode, similarly to the case where two particles overlap.

Our model was implemented in modern Fortran, utilizing a linked-cells algorithm for efficient neighbor searches as implemented in GeMS code.[25] The open source code for the project was named "dana" and is available at GitHub.[26] Simulations were performed with this code for at least 3,750,000 steps, corresponding to about 3.75 ms, depending on the simulation. Eight independent simulations were carried out for 15 $\rho$ values, ranging from $1 \cdot 10^{-4}$ to 1.0. The results presented here are averaged through independent simulations for each $\rho$, with the corresponding dispersion bars when needed.

## Results and discussion

Figure 1 shows representative configurations obtained from the present lithium deposition model at different probabilities $\rho$. As expected, dendritic growth is found to be larger as $\rho$ increases. This fact is related to the rate constants for electron transfer, $k^{TE}$, through

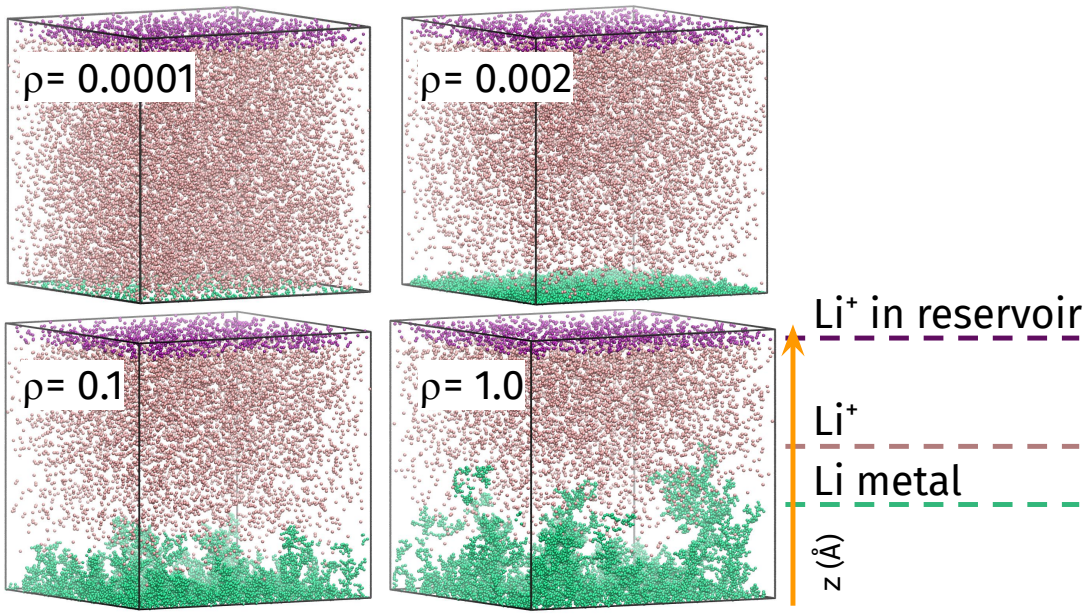


Figure 1: Final configurations of representative simulations lasting 3 ms approximately for different $\rho$ values. Green beads represent deposited Li atoms, while pink and violet correspond to $Li^+$ ions, with the violet ones being the ions inside the grand-canonical reservoir, as indicated by the labels.

Poisson distribution:

$$\rho = 1 - e^{k^{TE}(\eta)\Delta t} \tag{2}$$

Here, $\Delta t$ corresponds to a single time step of the molecular dynamics simulation during which electron transfer may occur with probability $\rho$. Since the electron transfer rate depends on the cell overpotential $\eta$,[27,28] a high $\rho$ probability is directly associated with a high overpotential,[16] so we will use both terms interchangeably. Note that our model is almost identical to that designed by Mayers *et al.*, although we use a planar electrode geometry instead of a spherical one. This difference has an important consequence: the ion concentration profile does not asymptotically converge as in spherical conditions.[28] In a planar electrode with no convection, ion depletion at the electrode surface due to deposition creates a concentration gradient that continuously advances towards the solution bulk. The gradient progression can be characterized by the increasing width of the Nernst diffusion layer, defined as $(2Dt)^{1/2}$.[29] Therefore, common computational approaches for

creating new ions to compensate for the consumed ones by deposition reaction[14,16,30] will eventually affect the progression of the concentration gradient, even if the ions are created as far away from the electrode as possible. This is also true for the grand canonical particle reservoir that we use in our simulations. To demonstrate this situation, the supporting information shows simulation results using a different reservoir mechanism designed to generate a minimum perturbation in the concentration of the ionic system. Figure S2 shows the rapid evolution of the concentration gradient towards the solution bulk. It is possible to conclude that the insertion of new ions at the top of the box will certainly perturb the diffusion layer evolution during our simulation times. Thus, it is crucial then to give a physical explanation for such perturbation.

In figure 2 we show the concentration profiles for $Li^+$ at different times during representative simulations. In this figure, it is possible to observe how the diffusion layer grows with time, as expected from the discussion above. However, note that the concentration gradient converges to a linear profile at longer times, maintaining the concentration of the bulk electrolyte for $z \geq 280$ Å due to the action of the reservoir. Note that the extent of the simulation box in the z-axis, *i.e.* perpendicular to the planar electrode, turns out to be an important parameter that regulates the concentration gradient during the deposition process. The described behavior is similar to that observed in a thin film electrode when the reactive species has reduced mobility inside the film relative to the electrolyte.[28,31] In a typical lithium metal battery, the diffusion coefficient in the solid electrolyte interphase (SEI) is about $10^{-14}$ $m^2/s$ while in DOL:DME it is around $10^{-10}$ $m^2/s$.[32,33] Therefore, it is reasonable to expect that the diffusion layer will not progress beyond the SEI/electrolyte interface, since it will be quickly compensated by the faster ions coming from the bulk. Thus, we will associate the plane between the reservoir region and the rest of our computational model with the interface existing in the real electrode between the electrolyte and the SEI. We argue here that the distance between the implicit electrode and the reservoir in this kind of model is directly related to the thickness of the SEI.

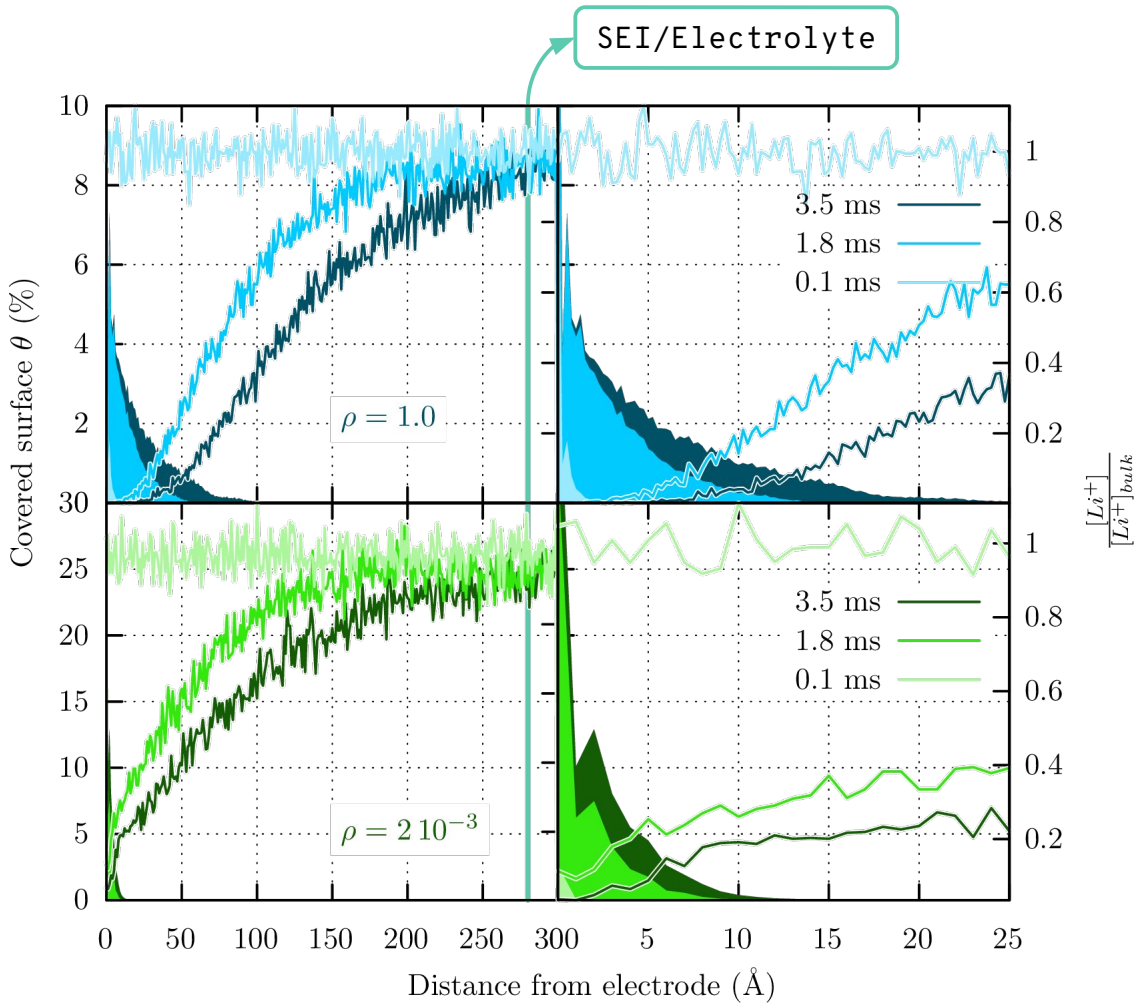


Figure 2: Relative $Li^+$ concentration profiles (lines, right axis) and electrode coverage percentages (filled areas, left axis) at three different deposition times and for two deposition probability $\rho$ values, given in the figure. $[Li^+]_{bulk} = 1$ M, and $\theta$ is in relative units to electrode geometrical area $A_{geom} = 9\ 10^{-11} cm^2$. The figures on the RHS are a zoom of the figures on the LHS between 0 and 25 Å.

We now quantify the extent of the metal growth due to the deposition reaction. In figure 2 we include the percentage of surface covered by the Li deposit, $\theta$, relative to the surface area of the bottom plane of the simulation box, *i.e.* the implicit electrode. In the upper part of this figure, we can see that, for the deposition probability of $\rho = 1$, the deposited lithium remains at low coverage percentages, below 8%, compared to those of $\rho = 0.002$, shown in the lower part of the figure, that reach 30% close to the electrode initial position. As the simulation time passes, lithium deposition mainly occurs in regions away from the electrode ($z > 20$ Å), while in closer regions ($z < 10$ Å) the coverage percentage remains almost invariant. This is coincident with the depletion of lithium ions available in these closer regions as shown by the ion concentration profiles. In fact, the dendritic growth is faster at the beginning of the simulations ($< 1.8$ ms) when more lithium ions are available. On the other hand, the decrease of $Li^+$ surface concentration is less abrupt for $\rho = 0.002$ and the covered surface close to the electrode is much higher. In this case, ion concentration at the electrode surface does not drop to zero and $\theta$ keeps growing there at longer simulation times.

One of the major consequences of dendritic growth is the increase in electrode surface area. A common quantity used to measure this increment is the electrode roughness factor, $f_r = A_{\text{real}}/A_{\text{geom}}$, where $A_{\text{real}}$ represents the true surface area that includes the dendrite contribution, and $A_{\text{geom}}$ is the geometrical area assuming a flat electrode surface.[29] For our simulation box $A_{\text{geom}} = 9\ 10^{-11}\text{cm}^2$. $A_{real}$ was computed using the solvent accessible surface area (SASA) algorithm included in VMD.[34,35] This algorithm works by counting random points on the surface of each atom, treated as a sphere of radius $r_{\text{SASA}}$, and then deleting those points that fall within their neighbors. This allows then for the calculation of the exposed surface of the dendritic structure as the simulation evolves. For this work, we have chosen the SASA radius of 3.2 Å, like the electron transfer reaction radius (see Simulation Methods section).

Figure 3a shows the average evolution of $f_r$ during deposition for different $\rho$ values.

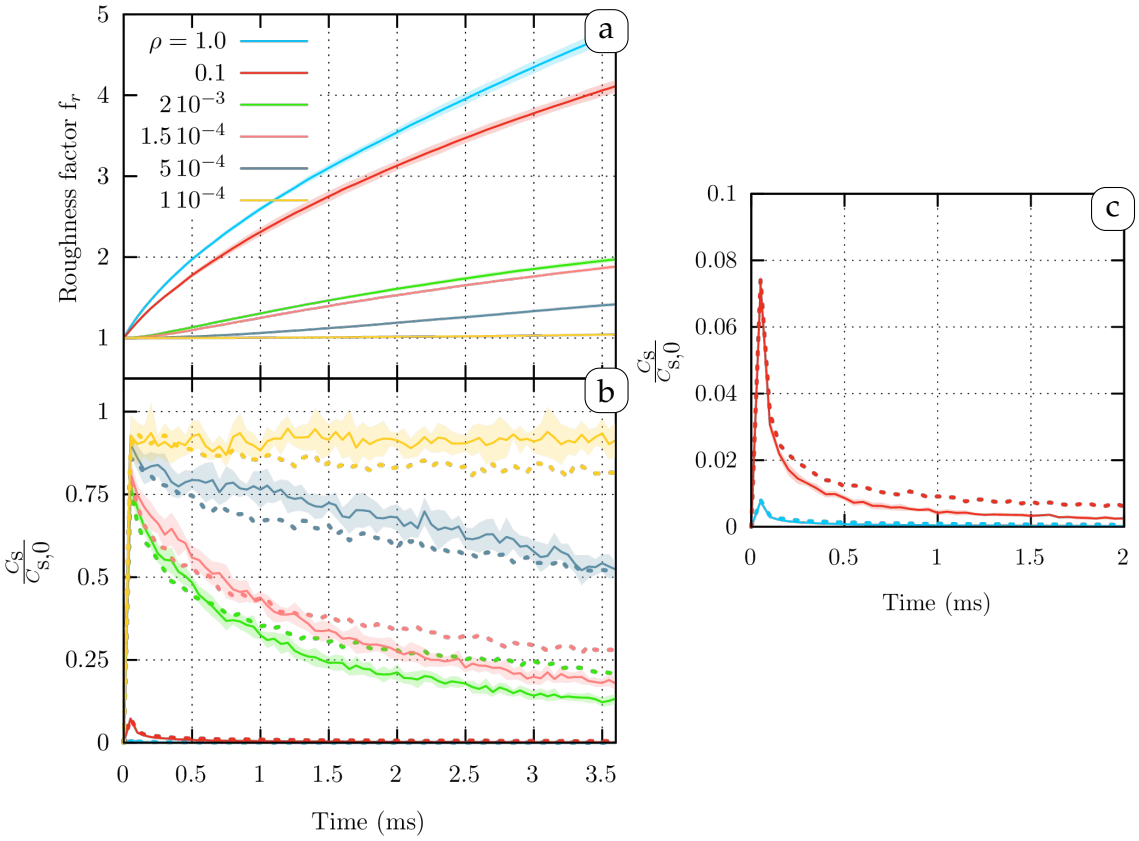


Figure 3: (a) Roughness factor along simulation time for different $\rho$ values, indicated in the figure, calculated as the ratio between the real area of the metal surface and the ideal electrode area as if it were flat. (b) The corresponding $Li^+$ surface concentration calculated as the number of deposition attempts. Also shown in dashed lines: the surface concentration obtained from simulations with inhibited dendrite growth. All curves correspond to averaged traces obtained from 8 simulation replicas. Standard deviation is indicated for solid lines using light shading. (c) A zoom showing the $Li^+$ surface concentration, for $\rho = 1.0$ and $\rho = 0.1$. The $C_s(0)$ value at the beginning of the simulation was $\approx 0.00763$ M/cm$^2$.

As expected, for high $\rho$ values the roughness factor grows larger and faster than for low $\rho$ values. This result shows that dendrite formation at high overpotentials can provoke the growth of the electrode area up to five times larger in just 3 ms of deposition. While the area increase observed in figure 3a is a direct consequence of the dendrite formation, it is not clear if this increase influences the number of ions that reach the surface. We calculated the $Li^+$ surface concentration, $C_s(t)$, at different $\rho$ as the number of deposition attempts on the electrode surface per unit of time, given that these attempts can only occur if the ion is at least 3.2 Å away from the electrode (see Simulation Methods section). The initial surface concentration before the start of deposition, $C_s(0) \approx 0.00763$ M/cm$^2$, is given by the bulk concentration ($C_b = 1$ M). The fluctuation of the relative surface concentration ($C_s(t)/C_s(0)$) due to the deposition reaction is shown in Figure 3b for different $\rho$. For low $\rho$ values the profile over time tends to be stationary, showing that ion diffusion compensates for the concentration drop caused by deposition. On the other hand, for higher overpotential (large $\rho$ values), there is a quick ion depletion characterized by a very small peak at the beginning of the simulations ($t < 0.5$ ms) followed by a fast drop to zero. Thus, based on the results shown in Figure 3, the influence of dendrites on deposition will depend on the balance between the increase in surface area and the decrease in surface concentration.

To further study the dendrite influence on surface concentration, we performed a set of simulations where dendrite formation was precluded. To do that, we modified the deposition scheme of the model: rather than turning the deposited ions into fixed lithium metal atoms, they were simply deleted from the simulation. With this condition, the evolution of electrode surface concentration (*i.e.* at $z = 0$ plane) was computed and depicted with dashed lines in figure 3b. Interestingly, despite the dendrite formation provoking a significant change in the electrode area, it does not drastically affect the surface concentration.

The current density can be computed from the number of lithium atoms deposited per

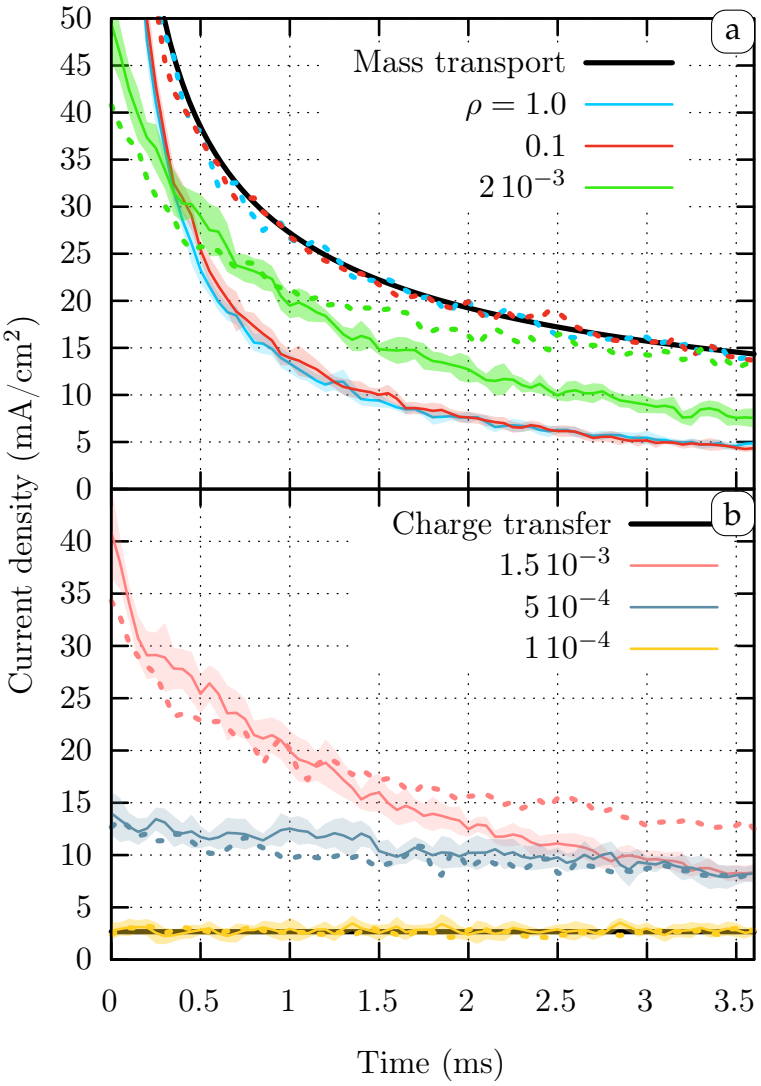


Figure 4: Current density profiles for different $\rho$ values. Solid lines are computed using equation 3. Dashed lines are computed from simulations with inhibited dendrite growth. All curves correspond to averaged traces obtained from 8 simulation replicas. Standard deviation is indicated for solid lines using light shading. Bold black lines correspond to limiting cases: (a) Cottrell equation 5, (b) equation 4 with $C_s = C_b$.

unit of time and area for different $\rho$ values:

$$j(t) = \frac{e}{A(t)} \frac{\mathrm{d}n_d(t)}{\mathrm{d}t} \tag{3}$$

where $n_d(t)$ is the number of particles deposited after a time $t$, counted from the beginning of the simulation, $e$ is the elementary charge constant and $A(t)$ is the electrode surface area. We have approximated this derivative with a middle point approximation, and the area is calculated, as before, with the SASA algorithm.

The resulting profiles are shown with solid lines in Figure 4 for some representative $\rho$ values. Each profile is an averaged $j(t)$ obtained using 8 simulation replicas. We include also in the figure a representation of the standard deviation associated with this average procedure. The individual current profiles for each replica for two representative $\rho$ values can be seen in the supporting information. We observe two distinct behaviors of current density. For $\rho$ greater than $\sim 10^{-3}$ the current shows an abrupt decay resembling the typical profile of a reaction limited by mass transport. As the $\rho$ values decrease, current profiles become more stable, or even constant ($\rho = 1\,10^{-4}$), exhibiting the typical behavior of a charge-transfer limited deposition.

Equation 3 can be rewritten using the charge-transfer constant as:[28,29]

$$j(t) = nFC_s(t)k^{TE} \tag{4}$$

where $C_s(t)$ is the surface concentration and $k^{TE}$ the electron transfer rate constant. Considering a roughness-free electrode surface, if the electron transfer rate is slow, $C_s(t)$ in equation 4 is expected to be close to $Li^+$ concentration at bulk, leading to a constant current density profile. On the other hand, for the limiting case of a very fast electron transfer reaction, deposition should be controlled by mass transport, as described by the well-known Cottrell equation:[28,29]

$$j(t) = nFC_b\sqrt{\frac{D}{\pi t}}\ , \tag{5}$$

where $F$ is the Faraday constant, $D$ is the diffusion coefficient, $C_b$ is the $Li^+$ concentration in the bulk and $n = 1$ is the number of electron transferred. This equation considers a roughness-free electrode surface in contact with a continuous semi-infinite electrolyte phase.

The current density profiles for $\rho = 1$, shown as blue continuous lines in Figure 4a, can be directly compared to the ideal Cottrell's prediction shown as a solid bold black line. As we did before, we have also included as dashed lines the results for simulations with inhibited dendrite growth. Note that for high $\rho$ values the latter profiles perfectly match the Cottrell profile ($\rho = 1,\ 0.1$, dashed lines), indicating that the main responsible for the deviation from ideal behavior is the dendrite growth. Note, however, that this agreement is limited to short times, since the reservoir induces a thin film scenario, as discussed before, leading to asymptotic behavior towards a positive current value different from the ideal zero limit. This asymptotic behavior can be seen in figure S4 of supporting information, where we show the results for longer simulation times.

Dendrite growth has two main consequences: the increase of the electrode area and the perturbation of the surface concentration. For the case of low potentials (low $\rho$), it is possible to observe in figure 4b that the dendrites induce only small differences in the current profiles. From equation 4, these differences can be directly attributed to the small differences in surface concentration with and without dendrite inhibition that have been shown in 3b. For the case of large potentials (high $\rho$), dendrites have a major influence in inducing a decrease in the current density relative to the Cottrellian case. Under these conditions, simulations are close to the limit where surface concentration tends to zero (figure 3c), so surface concentration cannot be associated with this effect. Therefore, the smaller values of the currents described by the blue and red full lines in figure 4 ($\rho = 1.0$ and $\rho = 0.1$) relative to the blue and red dotted lines are mainly determined by the large increase in surface area shown in figure 3a.

The theoretical treatment of a single-step chronoamperometry experiment using an

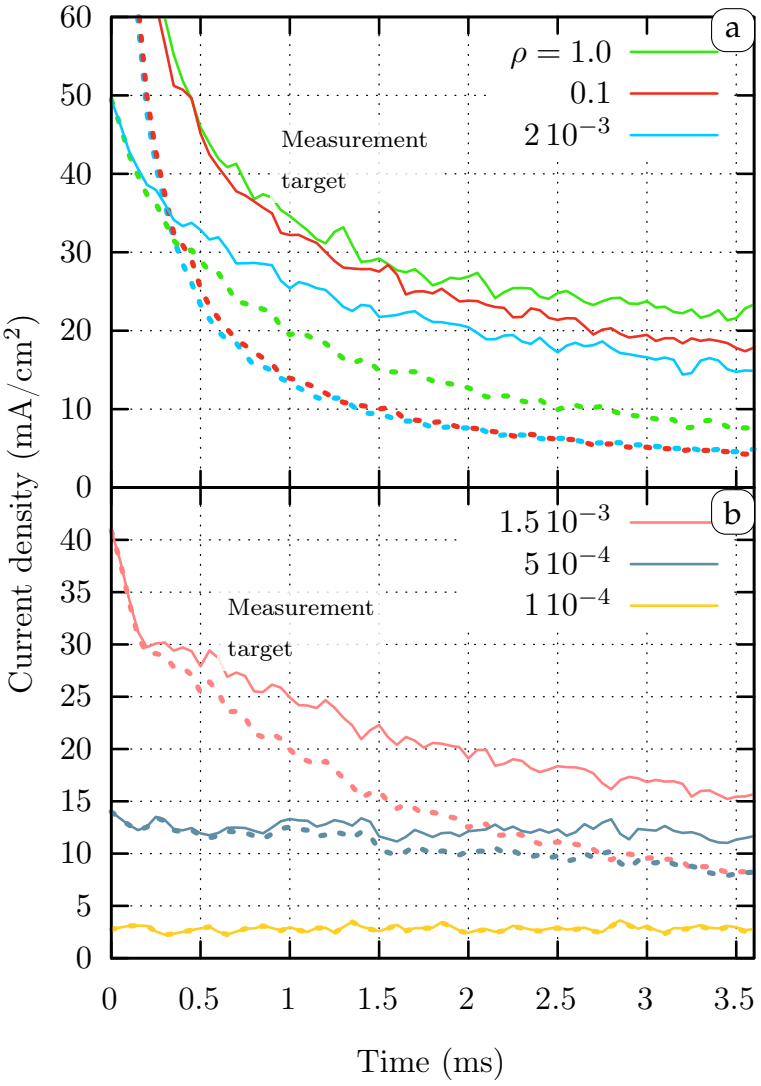


Figure 5: Same as figure 4, but dashed lines correspond to the density current profiles computed using equation 3 and considering a geometric surface area, $A_{geom}$, that ignores the increase of the electrode area given the growth of dendrites.

electrode with fractal roughness has been done by Pajkossy *et al.*[36–38] These authors use the different reactant equiconcentration surfaces as the different rulers or yardstick lengths used to measure the electrode surface area. This yardstick length can be used to find correlations between the fractal dimension of the electrode roughness and its electrochemical properties. In this same way, $r_{\mathrm{SASA}}$ can be regarded as a yardstick length used to compute the surface area. Note that however, our simulations imply a case of an electrode roughness that varies with time, starting with an initial value of $f_r = 1$ for a perfectly flat surface and followed by a constant growth. Using a particular yardstick length of $r_{\mathrm{SASA}} = 3.2$ allows us to understand the relative effect of the area increase due to dendrite presence. Even as an approximation to the real current density, simulations can serve as an important tool to extract information from simple experiments like the single-step chronoamperometry studied in this work. For instance, in Figure 5 we have included a set of current density profiles that were computed ignoring the real area of the electrode by approximating it with the geometric value, that is, $A(t) = A_{geom}$ in equation 3. This approximation is commonly used in electrochemical measurements due to the difficulty of accurately measuring the real area of the electrode during typical experiments. Therefore, we expect the experimental measurements to match the profiles depicted by the dashed lines in the figure. This is why we label these profiles as *measurement targets*. Note that these measurement targets deviate from both the ideal Cottrell behavior and the simulated one. However, we wish to remark that microscopic information can be better inferred from experiments by comparing the measurement results with the simulated profiles rather than the theoretical ones. For instance, the ratio between measurement profiles and simulated ones will certainly give a better approximation to the real electrode area. By changing $r_{\mathrm{SASA}}$, different yardstick lengths will be associated with such approximation.

# Conclusions

We built a coarse grained model to study lithium deposition on a planar electrode. Lithium ions are provided to the system through a grand canonical reservoir, which is placed at the end of the Solid Electrolyte Interface (SEI). Since this reservoir has an important influence on system behavior, its action was carefully analyzed from a theoretical point of view and also compared with a reservoir scheme with minimal system perturbation. We conclude that the differences in lithium-ion diffusion coefficients between the SEI and the bulk electrolyte generate an ion concentration gradient that remains confined to the SEI's extent. The SEI behaves as a thin film where ions diffuse slowly and its interface with the grand canonical reservoir corresponds to the boundary between the electrolyte and the SEI. This is a fundamental consideration to take into account when simulating the metal ion battery using planar electrode geometries.

Using this model we conducted simulations for chronoamperometry experiments, where a single-step potential is applied from starting equilibrium conditions. The evolution of the roughness factor, density current and ion concentration were monitored. Deviations from the Cottrell model due to dendrite presences were analyzed. Furthermore, by comparing the results with another set of simulations with deposit growth suppressed, we unveiled the influence of the dendrite formations on these quantities.

By using meaningful quantities with experimentally commonly used units, the present work does not only improve the understanding of coarse grain modeling for lithium batteries but also opens the possibility of direct comparison with experimental measures. For instance, we suggest a way to obtain the effective area of a real electrode by comparing the current density measurements of a coin cell with our simulated current density profiles. This could help to characterise more precisely dendritic growth in experimental systems since a more accurate estimation of the actual electrode surface area allows a better understanding of the electrochemical behaviour of lithium metal batteries.

## Acknowledgement

This work used computational resources from CCAD-UNC, which is part of SNCAD, Argentina. P. V. S. acknowledges her Ph.D. fellowship from CONICET. We acknowledge financial support from CONICET (28720210101190CO, 11220200102306CO, 1220200101189CO), Agencia Nacional de Promoción Científica y Tecnológica (PICT-2017-0621, 2020-SERIEA-03689) and SeCyT UNC (33820230100282CB, 33620180100980CB). We also acknowledge financial support from the bilateral cooperations between CNR (Italy) and CONICET (23020200100128CO) and between DST (India) and MinCyT (RESOL-2023-850-APNMCT).

## References

(1) Lin, D.; Liu, Y.; Cui, Y. Reviving the Lithium Metal Anode for High-Energy Batteries. *Nature Nanotechnology* **2017**, *12*, 194–206.

(2) Gao, M.; Li, H.; Xu, L.; Xue, Q.; Wang, X.; Bai, Y.; Wu, C. Lithium Metal Batteries for High Energy Density: Fundamental Electrochemistry and Challenges. *Journal of Energy Chemistry* **2021**, *59*, 666–687.

(3) Liu, T.; Vivek, J. P.; Zhao, E. W.; Lei, J.; Garcia-Araez, N.; Grey, C. P. Current Challenges and Routes Forward for Nonaqueous Lithium–Air Batteries. *Chemical Reviews* **2020**, *120*, 6558–6625.

(4) Chen, R.; Zhao, T.; Wu, F. From a Historic Review to Horizons beyond: Lithium–Sulphur Batteries Run on the Wheels. *Chemical Communications* **2015**, *51*, 18–33.

(5) Cheng, X.-B.; Zhang, R.; Zhao, C.-Z.; Zhang, Q. Toward Safe Lithium Metal Anode in Rechargeable Batteries: A Review. *Chemical Reviews* **2017**, *117*, 10403–10473.

(6) Gao, X.; Zhou, Y.-N.; Han, D.; Zhou, J.; Zhou, D.; Tang, W.; Goodenough, J. B. Thermodynamic Understanding of Li-Dendrite Formation. *Joule* **2020**, *4*, 1864–1879.

(7) Yuan, H.; Ding, X.; Liu, T.; Nai, J.; Wang, Y.; Liu, Y.; Liu, C.; Tao, X. A Review of Concepts and Contributions in Lithium Metal Anode Development. *Materials Today* **2022**, *53*, 173–196.

(8) Rao, X.; Lou, Y.; Zhong, S.; Wang, L.; Li, B.; Xiao, Y.; Peng, W.; Zhong, X.; Huang, J. Strategies for Dendrite-Free Lithium Metal Anodes: A Mini-review. *Journal of Electroanalytical Chemistry* **2021**, *897*, 115499.

(9) Santos, E.; Schmickler, W. The Crucial Role of Local Excess Charges in Dendrite Growth on Lithium Electrodes. *Angewandte Chemie International Edition* **2021**, *60*, 5876–5881.

(10) Fan, Y.; Chen, X.; Legut, D.; Zhang, Q. Modeling and Theoretical Design of Next-Generation Lithium Metal Batteries. *Energy Storage Materials* **2019**, *16*, 169–193.

(11) Lupo, C.; Schlettwein, D. Modeling of Dendrite Formation as a Consequence of Diffusion-Limited Electrodeposition. *Journal of The Electrochemical Society* **2019**, *166*, D3182–D3189.

(12) Selis, L. A.; Seminario, J. M. Dendrite Formation in Silicon Anodes of Lithium-Ion Batteries. *RSC Advances* **2018**, *8*, 5255–5267.

(13) Akolkar, R. Modeling Dendrite Growth during Lithium Electrodeposition at Sub-Ambient Temperature. *Journal of Power Sources* **2014**, *246*, 84–89.

(14) Kong, X.; Rudnicki, P. E.; Choudhury, S.; Bao, Z.; Qin, J. Dendrite Suppression by a Polymer Coating: A Coarse-Grained Molecular Study. *Adv Funct Materials* **2020**, *30*, 1910138.

(15) Nogales, P. M.; Lee, S.; Yang, S.; Jeong, S.-K. Effects of Electrolyte Solvent Composition on Solid Electrolyte Interphase Properties in Lithium Metal Batteries: Focusing on Ethylene Carbonate to Ethyl Methyl Carbonate Ratios. *Batteries* **2024**, *10*, 210.

(16) Mayers, M. Z.; Kaminski, J. W.; Miller, T. F. Suppression of Dendrite Formation via Pulse Charging in Rechargeable Lithium Metal Batteries. *The Journal of Physical Chemistry C* **2012**, *116*, 26214–26221.

(17) Aryanfar, A.; Brooks, D.; Merinov, B. V.; Goddard, W. A.; Colussi, A. J.; Hoffmann, M. R.; Colussi, J.; Ho, M. R.; Colussi, A. J.; Hoffmann, M. R. Dynamics of Lithium Dendrite Growth and Inhibition: Pulse Charging Experiments and Monte Carlo Calculations. *Journal of Physical Chemistry Letters* **2014**, *5*, 1721–1726.

(18) Aryanfar, A.; Brooks, D. J.; Colussi, A. J.; Merinov, B. V.; Goddard, W. A.; Hoffmann, M. R. Thermal Relaxation of Lithium Dendrites. *Physical Chemistry Chemical Physics* **2015**, *17*, 8000–8005.

(19) Aryanfar, A.; Cheng, T.; Colussi, A. J.; Merinov, B. V.; Goddard, W. A.; Hoffmann, M. R. Annealing Kinetics of Electrodeposited Lithium Dendrites. *Journal of Chemical Physics* **2015**, *143*.

(20) Byun, K.; Saha, J. K.; Jang, J. Role of a Solid–Electrolyte Interphase in the Dendritic Electrodeposition of Lithium: A Brownian Dynamics Simulation Study. *The Journal of Physical Chemistry C* **2020**, *124*, 9134–9141.

(21) Heffelfinger, G. S.; van Swol, F. Diffusion in Lennard-Jones Fluids Using Dual Control Volume Grand Canonical Molecular Dynamics Simulation (DCV-GCMD). *The Journal of Chemical Physics* **1998**, *100*, 7548.

(22) Papadopoulou, A.; Becker, E. D.; Lupkowski, M.; van Swol, F. Molecular Dynamics and Monte Carlo Simulations in the Grand Canonical Ensemble: Local versus Global Control. *The Journal of Chemical Physics* **1998**, *98*, 4897.

(23) Hubble, D.; Brown, D. E.; Zhao, Y.; Fang, C.; Lau, J.; McCloskey, B. D.; Liu, G. Liquid Electrolyte Development for Low-Temperature Lithium-Ion Batteries. *Energy & Environmental Science* **2022**, *15*, 550–578.

(24) Xu, K. Electrolytes and Interphases in Li-Ion Batteries and Beyond. *Chemical Reviews* **2014**, *114*, 11503–11618.

(25) Paz, S. A. GEMS is an Extensible Molecular Simulator. 2020. Publicly available at https://github.com/alexispaz/GEMS; Accessed: 2023-09-21.

(26) Saravia, P. V.; Paz, S. A. dana. 2023. Publicly available at https://github.com/pauvals/din-mol-li.

(27) Marcus, R. A.; Sutin, N. Electron Transfers in Chemistry and Biology. *Biochimica et Biophysica Acta (BBA) - Reviews on Bioenergetics* **1985**, *811*, 265–322.

(28) Bard, A. J.; Faulkner, L. R. *Electrochemical Methods: Fundamentals and Applications*, 2nd ed.; Wiley: New York, 2001.

(29) Bard, A. J.; Inzelt, G.; Scholz, F. *Electrochemical Dictionary*; Springer: Berlin, 2008.

(30) Choudhury, S.; Huang, Z.; Amanchukwu, C. V.; Rudnicki, P. E.; Chen, Y.; Boyle, D. T.; Qin, J.; Cui, Y.; Bao, Z. Ion Conducting Polymer Interfaces for Lithium Metal Anodes: Impact on the Electrodeposition Kinetics. *Advanced Energy Materials* **2023**, *13*, 2301899.

(31) Gerbino, L.; Baruzzi, A. M.; Iglesias, R. A. Catalytic EC′ Reaction at a Thin Film Modified Electrode. *Electrochimica Acta* **2013**, *88*, 66–73.

(32) Bergstrom, H. K.; Fong, K. D.; McCloskey, B. D. Interfacial Effects on Transport Coefficient Measurements in Li-ion Battery Electrolytes. *Journal of The Electrochemical Society* **2021**, *168*, 060543.

(33) Safari, M.; Kwok, C. Y.; Nazar, L. F. Transport Properties of Polysulfide Species in Lithium–Sulfur Battery Electrolytes: Coupling of Experiment and Theory. *ACS Central Science* **2016**, *2*, 560–568.

(34) Humphrey, W.; Dalke, A.; Schulten, K. VMD: visual molecular dynamics. *Journal of molecular graphics* **1996**, *14*, 33–38.

(35) Varshney, A.; Brooks, F. P.; Wright, W. V. Computing smooth molecular surfaces. *IEEE Computer Graphics and Applications* **1994**, *14*, 19–25.

(36) Pajkossy, T. Electrochemistry at Fractal Surfaces. *Journal of Electroanalytical Chemistry and Interfacial Electrochemistry* **1991**, *300*, 1–11.

(37) Pajkossy, T.; Borosy, A.; Imre, A.; Martemyanov, S.; Nagy, G.; Schiller, R.; Nyikos, L. Diffusion Kinetics at Fractal Electrodes. *Journal of Electroanalytical Chemistry* **1994**, *366*, 69–73.

(38) Pajkossy, T. *Encyclopedia of Interfacial Chemistry*; Elsevier, 2018; pp 121–124.